

Superconducting and normal-state properties of the noncentrosymmetric superconductor Re_6Zr

D. A. Mayoh,^{1,*} J. A. T. Barker,^{1,†} R. P. Singh,² G. Balakrishnan,¹ D. McK. Paul,¹ and M. R. Lees^{1,‡}

¹*Physics Department, University of Warwick, Coventry, CV4 7AL, United Kingdom*

²*Department of Physics, Indian Institute of Science Education and Research Bhopal, Bhopal 462066, India*

We systematically investigate the normal and superconducting properties of non-centrosymmetric Re_6Zr using magnetization, heat capacity, and electrical resistivity measurements. Resistivity measurements indicate Re_6Zr has poor metallic behavior and is dominated by disorder. Re_6Zr undergoes a superconducting transition at $T_c = (6.75 \pm 0.05)$ K. Magnetization measurements give a lower critical field, $\mu_0 H_{c1} = (10.3 \pm 0.1)$ mT. The Werthamer-Helfand-Hohenberg model is used to approximate the upper critical field $\mu_0 H_{c2} = (11.2 \pm 0.2)$ T which is close to the Pauli limiting field of 12.35 T and which could indicate singlet-triplet mixing. However, low-temperature specific-heat data suggest that Re_6Zr is an isotropic, fully gapped s -wave superconductor with enhanced electron-phonon coupling. Unusual flux pinning resulting in a peak effect is observed in the magnetization data, indicating an unconventional vortex state.

I. INTRODUCTION

In superconductors, the inversion symmetry of the crystallographic structure plays a central role in the formation of the Cooper pairs. In conventional superconductors, each Cooper pair is formed from two electrons which belong to the same Fermi surface with a symmetric orbital state and an antisymmetric spin state. The discovery of superconductivity in CePt_3Si , a material which lacks inversion symmetry, has generated considerable experimental and theoretical interest in the physics of noncentrosymmetric (NCS) superconductors¹⁻³. The absence of inversion symmetry in NCS materials introduces an antisymmetric spin-orbit coupling^{4,5} which can result in a splitting of the spin-up and spin-down conduction electron energy bands. This splitting of the Fermi surface, lifting the degeneracy of the conduction electrons, may result in a superconducting pair wave function that is an admixture of spin-singlet and spin-triplet states, although there are several examples of NCS superconductors where it has been established that the order parameter is not unconventional, for example, BiPd ⁶ and PbTaSe_2 ⁷. Singlet-triplet mixing can lead NCS materials to display significantly different properties from conventional superconducting systems, for example, the triplet pairing seen in $\text{Li}_2(\text{Pd,Pt})_3\text{Si}$ ⁸⁻¹¹, and upper critical fields close to or exceeding the Pauli limiting field observed in $\text{Mo}_3\text{Al}_2\text{C}$ ^{12,3}, Re_3W ¹³, $\text{Ca}(\text{Ir,Pt})\text{Si}_3$ ¹⁴, $\text{Li}_2(\text{Pd,Pt})_3\text{Si}$ ⁸⁻¹¹, LaRhSi_3 ¹⁵, $\text{Nb}_{0.18}\text{Re}_{0.82}$ ¹⁶, Y_2C_3 ¹⁷, and $\text{Mg}_{10}\text{Ir}_{19}\text{B}_{16}$ ¹⁸.

Noncentrosymmetric superconductors are prime candidates to exhibit time-reversal symmetry (TRS) breaking. Until recently, however, this rare phenomenon had been observed directly in only a few unconventional centrosymmetric superconductors, for example, $\text{PrPt}_4\text{Ge}_{12}$ ¹⁹, Sr_2RuO_4 ^{20,21}, $(\text{Pr,Lu})(\text{Os,Ru})_4\text{Sb}_{12}$ ^{22,23}, UPt_3 and $(\text{U,Th})\text{Be}_{13}$ ²⁴⁻²⁷, and LaNiGa_2 ²⁸ and the cage-type superconductors $\text{Lu}_5\text{Rh}_6\text{Sn}_{18}$ ²⁹, while no spontaneous magnetization associated with TRS breaking had been reported in any of the NCS materials mentioned above.

Recently, this situation has changed, and several NCS superconductors have been reported to show TRS breaking. In the first of these, LaNiC_2 , symmetry analysis implies that the superconducting instability is of the nonunitary triplet type, with a spin-orbit coupling that is comparatively weak and with mixing of singlet and triplet pairing being forbidden by symmetry^{30,31}. TRS breaking was also found in La_7Ir_3 , with measurements of the superconducting gap indicating that it is isotropic with a superconducting ground state that is dominated by an s -wave component³².

Re_6Zr is a member of the α -Mn family of intermetallic compounds³³ and has a noncentrosymmetric cubic structure, space group $I\bar{4}3m$. We have previously reported the results of muon spin relaxation (μSR) measurements on Re_6Zr , showing that TRS is broken in this material. A theoretical analysis of the possible pairing states demonstrated that a mixing of spin-singlet and spin-triplet pairing is possible in this noncentrosymmetric superconducting compound^{33,34}. Here, we present a comprehensive characterization of the normal and superconducting states of this intermetallic compound through studies by magnetization, electronic transport, and heat capacity. We estimate several normal state parameters of Re_6Zr such as the electronic specific-heat contribution γ_n , residual resistivity ρ_0 , and the hyperfine contribution to the specific heat. Using the electronic-transport and heat-capacity measurements, we estimate the Debye temperature by using the parallel-resistor model, the Debye lattice contribution to the specific heat at low temperature, and the Debye-Einstein model. Several superconducting parameters, including the lower and upper critical fields H_{c1} and H_{c2} , the coherence length ξ_{GL} , and the penetration depth λ_{GL} , are estimated. The specific-heat jump $\Delta C/\gamma_n T_c$, the superconducting gap $\Delta_0/k_B T_c$, and the temperature dependence of the specific heat at low-temperature suggest that Re_6Zr is an isotropic, fully gapped s -wave superconductor with enhanced electron-phonon coupling. We also present evidence of unusual flux pinning not normally seen in low- T_c systems.

II. EXPERIMENTAL DETAILS

Polycrystalline samples of Re_6Zr were prepared by arc melting stoichiometric quantities of high-purity (4N) Zr and Re in an arc furnace under an argon (5N) atmosphere on a water-cooled copper hearth. The sample buttons were melted and flipped several times to ensure phase homogeneity. The observed weight loss during the melting was negligible. Powder x-ray diffraction data confirmed the α -Mn crystal structure and the phase purity of the samples. A low ($\chi_{\text{dc}} = 5.8 \times 10^{-4}$), nearly temperature independent normal-state dc susceptibility indicates there are no magnetic impurities from the Zr.

The normal and superconducting states of Re_6Zr were characterized by magnetization M , ac susceptibility χ_{ac} , ac resistivity ρ , and heat capacity C measurements. The dc magnetization measurements were performed as a function of temperature T at fixed field or as a function of applied magnetic field $\mu_0 H$ at a fixed temperature in a Quantum Design Magnetic Property Measurement System (MPMS) magnetometer in temperatures ranging from 1.8 to 300 K and under magnetic fields up to 5 T. The ac susceptibility measurements were also performed in a Quantum Design MPMS with an ac applied field of 0.3 mT and a frequency of 30 Hz in dc magnetic fields up to 5 T. For field-dependent magnetization studies an Oxford Instruments vibrating sample magnetometer (VSM) was used with magnetic fields up to 10 T. Heat capacity was measured using a two-tau relaxation method in a Quantum Design Physical Property Measurement System (PPMS) at temperatures ranging from 1.9 to 300 K in magnetic fields up to 8 T. Lower-temperature measurements down to 0.5 K were carried out with a ^3He insert. The samples were attached to the measuring stage using Apiezon[®] N grease to ensure good thermal contact. Electrical resistivity measurements were made using a conventional four-probe ac technique with a measuring frequency of 113 Hz and a current of 5.1 mA in a Quantum Design PPMS. The measurements were performed at temperatures ranging from 1.9 to 300 K in magnetic fields up to 9 T. The shape of the sample used for the majority of the measurements was a rectangular prism to allow the demagnetization factor to be evaluated³⁵ and minimized along one direction.

III. RESULTS AND DISCUSSION

A. Electrical resistivity

Figure 1(a) shows the resistivity as a function of temperature $\rho(T)$ of a polycrystalline Re_6Zr sample from 2 to 300 K in zero field. The small value of the residual resistivity ratio, $\text{RRR} \equiv \rho(300 \text{ K})/\rho(10 \text{ K}) \approx 1.09$, and the high normal-state resistivity at 10 K indicate poor metallic behavior. This is comparable to other Re compounds such as Re_6Hf with a RRR quoted from 1.08 to 1.4^{36,37}, $\text{Re}_{24}\text{Ti}_5$ with $\text{RRR} \sim 1.3$ ³⁸, and $\text{Nb}_{0.18}\text{Re}_{0.82}$

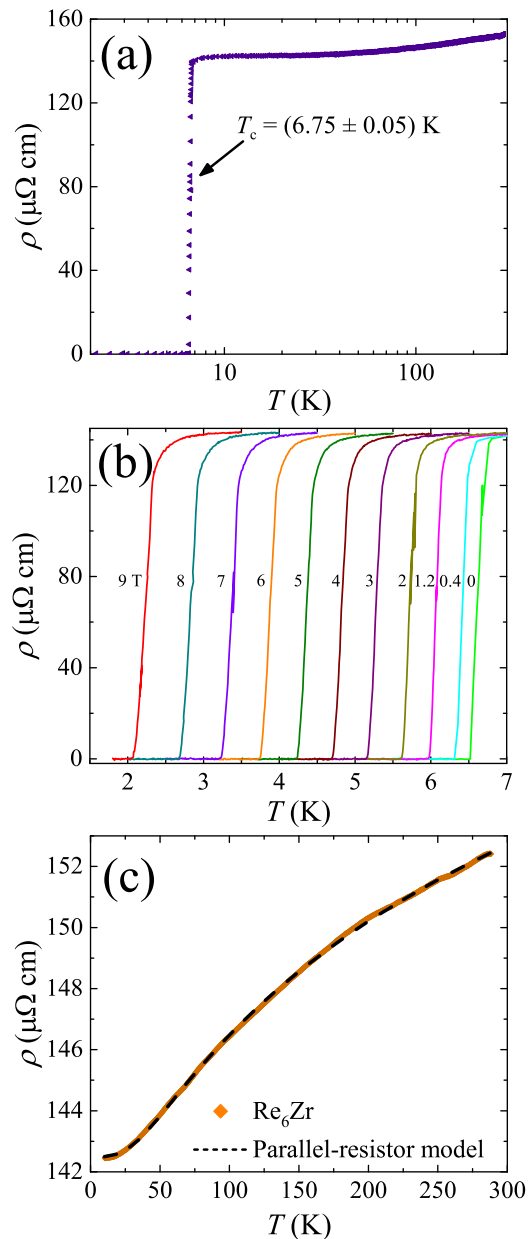


FIG. 1: (a) Resistivity versus temperature $\rho(T)$ of Re_6Zr in the range $1.8 \leq T \leq 250$ K measured in zero applied magnetic field. The midpoint of the resistivity drop was taken as the transition temperature. (b) $\rho(T)$ below 7.5 K shows the suppression of the transition temperature under various applied fields $\mu_0 H$ from 0 to 9 T. (c) $\rho(T)$ data in the normal state fitted with the parallel-resistor model over the temperature range 10 to 290 K.

with $\text{RRR} \sim 1.3$ ¹⁶. A sharp, zero-field superconducting transition ($\Delta T_c = 0.20$ K) can be seen clearly in Fig. 1(b) at $T_c = (6.76 \pm 0.05)$ K. T_c is gradually suppressed with increasing applied magnetic field [see Fig. 1(b)] and the transition is broadened so that $\Delta T_c = 0.28$ K at 9 T.

At temperatures greater than ~ 50 K the $\rho(T)$ of Re_6Zr is seen to flatten. This characteristic is similar

to that seen in many superconductors containing d-block elements including BiPd³⁹. It has been proposed that in certain compounds at high temperatures the resistivity saturates at a value that corresponds to the mean free path on the order of the inter-atomic spacing⁴⁰. This idea was further developed by Wiesmann *et al.*⁴¹ who found empirically that $\rho(T)$ could be described by the parallel-resistor model:

$$\rho(T) = \left[\frac{1}{\rho_{\text{sat}}} + \frac{1}{\rho_{\text{ideal}}(T)} \right]^{-1}, \quad (1a)$$

where ρ_{sat} is the saturated resistivity at high temperatures and is independent of T , and $\rho_{\text{ideal}}(T)$ is the “ideal” contribution which according to Matthiessen’s rule is:

$$\rho_{\text{ideal}}(T) = \rho_{\text{ideal},0} + \rho_{\text{ideal},L}(T). \quad (1b)$$

Here $\rho_{\text{ideal},0}$ is the ideal temperature-independent residual resistivity and $\rho_{\text{ideal},L}(T)$ is the temperature-dependent contribution which can be expressed by the generalized Bloch-Grüneisen model⁴²

$$\rho_{\text{ideal},L}(T) = C \left(\frac{T}{\Theta_R} \right)^n \times \int_0^{\Theta_R/T} \frac{x^n}{(e^x - 1)(1 - e^{-x})} dx, \quad (1c)$$

where Θ_R is the Debye temperature obtained from resistivity measurements, C is a material-dependent prefactor and $n = 3 - 5$ depending on the nature of the carrier scattering. Fig. 1(c) shows the normal-state resistivity data from 10 to 290 K fit using Eq. 1a. It was found that a value of $n = 3$, which takes into account umklapp scattering between bands, achieved the best fit giving $\rho_{\text{sat}} = (167 \pm 2) \mu\Omega \text{ cm}$, $C = (315 \pm 6) \mu\Omega \text{ cm}$ and $\Theta_R = (237 \pm 2) \text{ K}$. The measured residual resistivity, $\rho_0 = (142 \pm 2) \mu\Omega \text{ cm}$, which is related to $\rho_{\text{ideal},0}$ and ρ_{sat} by

$$\rho_0 = \frac{\rho_{\text{ideal},0}\rho_{\text{sat}}}{\rho_{\text{ideal},0} + \rho_{\text{sat}}}, \quad (2)$$

is consistent with the values of the fit. This electrical resistivity data is in close agreement with that previously reported in Ref. 43.

B. Heat capacity

The temperature dependence of the heat capacity divided by temperature, C/T , versus T^2 from 2 to 10 K is shown in Fig. 2(a), where a sharp jump at $(6.75 \pm 0.05) \text{ K}$ indicates a bulk superconducting transition. The sharpness of this peak gives an indication of the high quality of the sample. We analyzed the normal-state data C/T versus T^2 between 4.4 and 10 K at $\mu_0 H = 0 \text{ T}$ using

$$C/T = \gamma_n + \beta_3 T^2 + \beta_5 T^4, \quad (3)$$

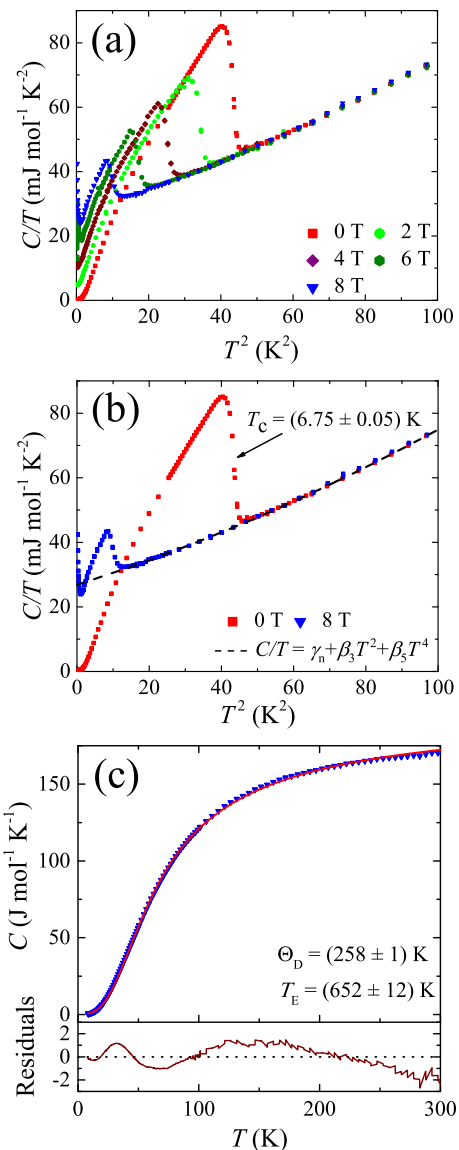


FIG. 2: (a) C/T versus T^2 in different applied fields ($\mu_0 H$ in teslas), showing the suppression in T_c for increasing field. (b) C/T versus T^2 with $\mu_0 H = 0$ and 8 T . The line is a fit using $C/T = \gamma_n + \beta_3 T^2 + \beta_5 T^4$ for all the $C(T)$ data collected above $T_c(H)$ in the different applied fields. The normal-state electronic contribution to the specific heat $\gamma_n = (26.9 \pm 0.1) \text{ mJ mol}^{-1} \text{ K}^{-2}$, and the Debye temperature $\Theta_D = (338 \pm 9) \text{ K}$. (c) C versus T from 10 to 300 K. The line shows the fit using Eq. (5a), the Debye-Einstein function. The residual plot underneath indicates the quality of the fit using the Debye-Einstein function to the data.

where γ_n is the normal state Sommerfeld electronic-heat-capacity contribution, β_3 is the Debye law lattice-heat-capacity contribution, and β_5 is from higher order lattice contributions. A fit using Eq. (3) can be seen in Fig. 2(b) which gives $\gamma_n = (26.9 \pm 0.1) \text{ mJ mol}^{-1} \text{ K}^{-2}$, $\beta_3 = (0.35 \pm 0.02) \text{ mJ mol}^{-1} \text{ K}^{-4}$ and $\beta_5 = (1.2 \pm 0.3) \mu\text{J mol}^{-1} \text{ K}^{-6}$. The Debye tem-

perature, Θ_D , can then be calculated using

$$\Theta_D = \left(\frac{12\pi^4 RN}{5\beta} \right)^{1/3}, \quad (4)$$

where R is the molar gas constant and N is the number of atoms per unit cell. Eq. 4 gives $\Theta_D = (338 \pm 9)$ K which is slightly higher than the previously reported value³⁴.

Figure 2(c) shows the temperature dependence of the heat capacity up to 300 K. There is no sign of any structural phase transition, and the value of C at 300 K is $169.5 \text{ J mol}^{-1} \text{ K}^{-1}$, which is close to classical Dulong-Petit value for Re_6Zr of $174.6 \text{ J mol}^{-1} \text{ K}^{-1}$ and is consistent with $\Theta_D > 300$ K. We fit the normal-state data using a Debye-Einstein function. It was found that by including the additional Einstein term to the Debye model for lattice heat capacity the fit could be significantly improved. Figure 2(c) shows heat-capacity data from 10 to 300 K, which was fit with⁴⁴

$$C(T) = \gamma_n T + n\delta C_{\text{Debye}} \left(\frac{T}{\Theta_D} \right) + n(1 - \delta) C_{\text{Einstein}} \left(\frac{T}{T_E} \right), \quad (5a)$$

where δ is the fractional contribution of C_{Debye} , n is the number of atoms in a formula unit (f.u.), C_{Debye} is given by

$$C_{\text{Debye}} \left(\frac{T}{\Theta_D} \right) = 9R \left(\frac{T}{\Theta_D} \right)^3 \int_0^{\Theta_D/T} \frac{x^4 e^x}{(e^x - 1)^2} dx, \quad (5b)$$

and C_{Einstein} is given by

$$C_{\text{Einstein}} \left(\frac{T}{T_E} \right) = 3R \frac{z^2 e^z}{(e^z - 1)^2}, \quad (5c)$$

where $z = T_E/T$ and T_E is the Einstein temperature. The fit was performed using a fixed value $\gamma_n = 26.9 \text{ mJ mol}^{-1} \text{ K}^{-2}$ to help reduce the number of free parameters. We obtained $\delta = 0.912 \pm 0.002$, $\Theta_D = (258 \pm 1)$ K, and $T_E = (652 \pm 12)$ K. The difference between Θ_D and Θ_R is also expected due to the limitations of the parallel-resistor model.

In Fig. 2, at very low temperatures, an upturn in C/T appears in magnetic fields above 6 T. This anomalous contribution to the specific heat is proportional to T^{-2} , which suggests that it is due to the high-temperature tail of a nuclear Schottky anomaly. The specific heat of the measured Re_6Zr can be expressed as

$$C(T, B) = C_{\text{el}}(T, B) + C_{\text{ph}}(T) + C_{\text{hf}}(T, B), \quad (6)$$

where C_{el} is the electronic contribution, C_{hf} is the Schottky contribution, and C_{ph} is the phonon contribution. The high-temperature approximation of the nuclear hyperfine contribution to the specific heat was modeled by $C_{\text{hf}} = A_0 T^{-2}$, where A_0 is a field-dependent parameter.

A_0 is estimated to be $\sim 1.4 \text{ mJ K mol}^{-1}$ at 8 T, which is consistent with the value previously obtained for pure rhenium^{45,46}. The results of this analysis raise a note of caution.

A hyperfine contribution to the specific heat has also been seen in other Re-based α -Mn compounds, $\text{Nb}_{0.18}\text{Re}_{0.82}$ ⁴⁷ and Re_6Hf ³⁷, as well as in pure Re^{45,46}, indicating that a Schottky anomaly may always be present in Re-based superconductors at low temperatures. Mazidian *et al.* demonstrated that in order to establish the presence of point or line nodes in the superconducting gap, the heat capacity needs to be fit below $T_c/10$ ⁴⁸. Modifications by a magnetic field below T_c to both $C_{\text{el}}(T, B)$ and $C_{\text{hf}}(T, B)$ mean that a precise evaluation of the temperature dependence of the electronic specific heat and hence the gap structure in all Re-based NCS superconductors, including those with an α -Mn structure, may be challenging, as this will require an accurate evaluation of the hyperfine contribution to the specific heat.

C. Magnetization and lower critical field

Figure 3(a) shows the dc susceptibility data $\chi_{\text{dc}}(T)$ taken in zero-field-cooled warming (ZFCW) and field-cooled cooling (FCC) modes in an applied field of 1 mT. These data confirm that Re_6Zr is a superconductor with $T_c = (6.70 \pm 0.05)$ K. The sample exhibits a full Meissner fraction for the ZFCW. There is almost no flux expulsion on re-entering the superconducting state during FCC. The strong pinning is consistent with a disordered system. Magnetization versus field sweeps in low fields (0 to 16 mT) at several temperatures are shown in Fig. 3(b). The lower critical field, $H_{c1}(T)$, is determined from the first deviation from linearity of the initial slope as the field is increased. In Fig. 3(c) the resulting $H_{c1}(T)$ values are plotted against temperature. Ginzburg-Landau (GL) theory gives

$$H_{c1}(T) = H_{c1}(0) \left[1 - \left(\frac{T}{T_c} \right)^2 \right]. \quad (7)$$

Fitting the data using Eq. (7), $H_{c1}(0)$ was estimated to be (10.3 ± 0.1) mT.

The ac susceptibility versus temperature measurements $\chi_{\text{ac}}(T)$ shown in Fig. 4 confirm the superconducting transition of $T_c = (6.70 \pm 0.05)$ K. In dc bias fields less than $H_{c1}(0)$ the sample exhibits a full Meissner fraction. The out-of-phase component of the ac susceptibility $\chi''(T)$ contains a sharp maximum close to T_c and falls to zero for lower temperatures. This is consistent with the strong flux pinning seen in the low-field FCC $M(T)$ data. For applied fields much greater than $H_{c1}(0)$, T_c is suppressed, and a full Meissner fraction is not seen due to partial flux penetration. An anomalous dip can be seen close to T_c , suggesting flux is being reexpelled from the sample due to unusual flux dynamics. At lower tempera-

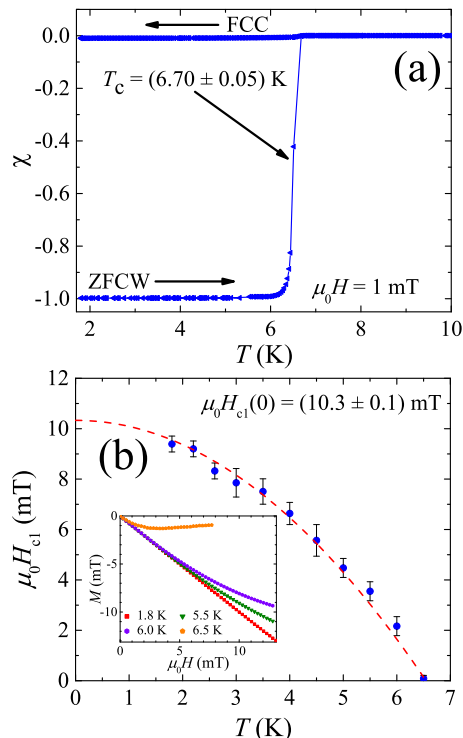


FIG. 3: (a) Temperature dependence of the dc magnetic susceptibility $\chi_{dc}(T)$ collected in zero-field-cooled warming (ZFCW) and field-cooled cooling (FCC) modes in an applied field of $\mu_0H = 1$ mT. (b) Lower critical field H_{c1} versus temperature for Re_6Zr . The H_{c1} values were taken as the fields at which initial magnetization versus field data shown in Fig. 3(b) first deviate from linearity (as shown in the inset). The solid line shows the fit using Eq. (7) giving $\mu_0H_{c1}(0) = (10.3 \pm 0.1)$ mT.

ture, $\chi''(T)$ exhibits a broad maximum, indicating losses due to flux motion in dc applied fields $\mu_0H \geq 2$ T.

Further evidence of unusual flux pinning in Re_6Zr can be seen in the $M(H)$ loops taken in the both the superconducting quantum interference device (SQUID) magnetometer and the VSM (see Fig. 5), suggesting that the observed features cannot simply be attributed to the significant movement of the sample in a magnetic field or the magnetic field sweep rate. As is evident from Fig. 5(a), above H_{c1} , Re_6Zr exhibits the conventional behavior for a type-II superconductor, with a hysteresis in the magnetization ΔM decreasing with increasing temperature and magnetic field. For applied fields close to $H_{c2}(T)$ this hysteresis ΔM disappears, and the magnetization becomes reversible as vortices appear to become unpinned. The inset in Fig. 5(a) shows how this irreversibility field H_{irr} varies with temperature. These data were collected using a plate-shaped sample with the field applied in the plane of the plate, i.e., with the demagnetization factor of the sample minimized. By changing the sample orientation with respect to the applied field a change in vortex pinning is observed, as can be seen in Figs. 5(b) and 5(c), where the demagnetization factor was maxi-

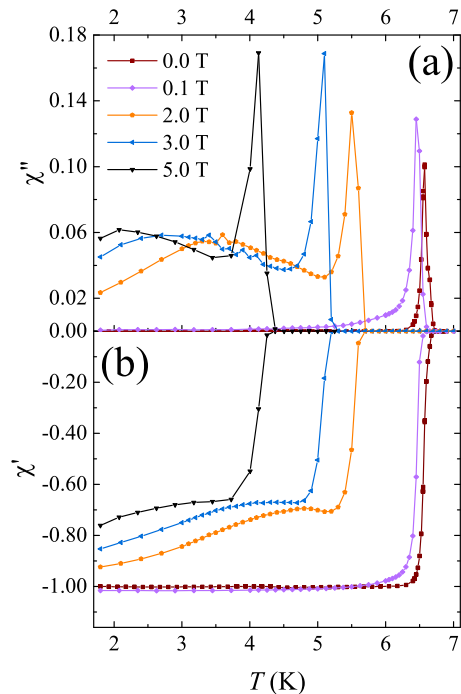


FIG. 4: (a) Imaginary part of ac susceptibility versus temperature $\chi''(T)$ in various dc applied fields. (b) Real part of ac susceptibility versus temperature $\chi'(T)$ at various dc applied fields. In zero dc field, a sharp superconducting transition can be seen at (6.70 ± 0.05) K. In fields above $H_{c1}(0)$ an anomalous dip in the magnetization is seen close to the transition temperature.

mized. In Figs. 5(b) and 5(c) a clear secondary maximum (fishtail) is observed. As the sample is cooled, there is a slight shift to higher magnetic field in the onset and the peak of the fishtail. This behavior is not normally observed in low- T_c superconductors but is quite common in the high- T_c oxides and in some two-dimensional superconducting materials, indicating unconventional vortex states. The symmetry of the hysteresis in the field-increasing and field-decreasing legs of the $M(H)$ curves suggests that bulk pinning rather than surface barriers may be the dominant mechanism leading to the fishtail. Assuming the superconducting critical current is proportional to ΔM , the maximum pinning force in the field range 1 to 3 T, as reflected in the fishtail, appears to be almost temperature independent between 3 and 5 K. It is suggested that the unusual vortex states arise from the normal pinning centers such as grain boundaries within the sample. A detailed study on the vortex states in high-quality single crystals of Re_6Zr is needed to explore the vortex physics further.

D. Superconducting gap

The jump in specific heat in zero field indicates the onset of bulk superconductivity. The transition temper-

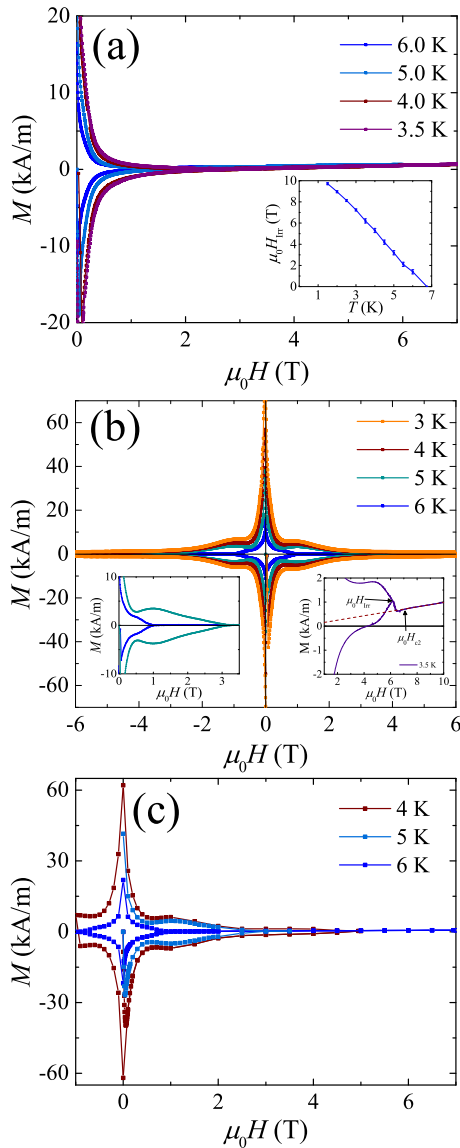


FIG. 5: (a) Magnetization vs magnetic field at several temperatures for Re_6Zr . The data were collected in a VSM on a plate-shaped sample with the demagnetization factor of the sample minimized. The inset shows how H_{irr} varies with temperature. (b) Magnetization vs. magnetic field at several temperatures collected in a vibrating sample magnetometer with the demagnetization factor of the Re_6Zr sample maximized. A secondary maximum (fish-tail) can clearly be seen in the magnetization at around 1.25 T. The left inset shows the 5 and 6 K curves between 0 and 3.5 T. H_{irr} and H_{c2} are indicated in the right inset showing the 3.5 K curve between 2 and 10 T. (c) Magnetization vs magnetic field at several temperatures collected in the SQUID magnetometer. The fish-tail can also be clearly seen in a magnetic field of ~ 1.25 T.

ature is defined as the midpoint of the transition, giving $T_c = (6.75 \pm 0.05)$ K. The data in Fig. 6(a) were fit using the BCS model of the specific heat given in Ref. 49. The

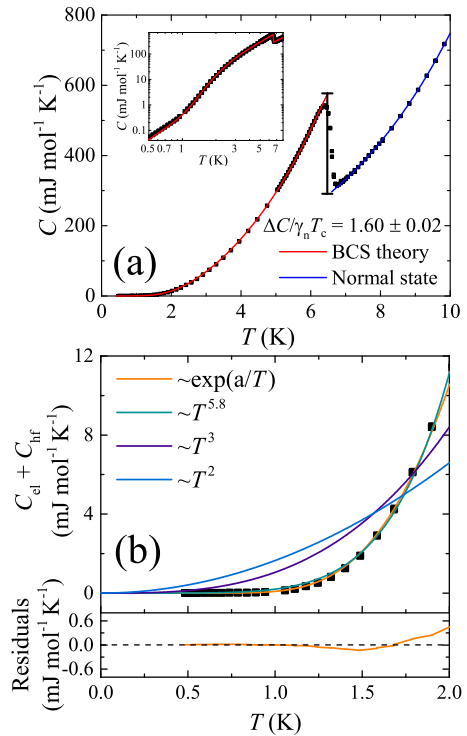


FIG. 6: (a) Heat capacity versus temperature in zero field for Re_6Zr across the superconducting transition. The red line shows a fit across the superconducting transition for a fully gapped superconductor as described in Sec. III D. The inset shows the heat capacity across the superconducting transition on a log-log scale. From this it can be seen that the data are very well fit by the isotropic s -wave BCS model. (b) Electronic heat capacity C_{el} versus temperature below 2.5 K showing various power laws (anisotropic gap) and an exponential (isotropic gap) fit to the low-temperature data. The χ^2 and residuals shown are for the exponential fit.

entropy S was calculated from

$$\frac{S}{\gamma_n T_c} = -\frac{6}{\pi^2} \frac{\Delta_0}{k_B T_c} \int_0^\infty [f \ln f + (1-f) \ln(1-f)] dy, \quad (8)$$

where f is the Fermi-Dirac function given by $f = [1 + \exp(E/k_B T)]^{-1}$ and $E = \Delta_0 \sqrt{y^2 + \delta(T)^2}$, where y is the energy of the normal-state electrons and $\delta(T)$ is the temperature dependence of the superconducting gap calculated from the BCS theory. The specific heat of the superconducting state is then calculated by

$$\frac{C_{\text{sc}}}{\gamma_n T_c} = T \frac{d(S/\gamma_n T_c)}{dT}. \quad (9)$$

The superconducting gap $\Delta_0/k_B T_c$ was estimated to be 1.86 ± 0.05 , which is in agreement with Ref. 34. For conventional BCS superconductors a value of 1.76 is expected, and the larger value for Re_6Zr indicates that the electron-phonon coupling is slightly enhanced. $\Delta C/\gamma_n T_c = 1.60 \pm 0.02$ is also larger than the 1.43 expected for conventional BCS superconductors and agrees

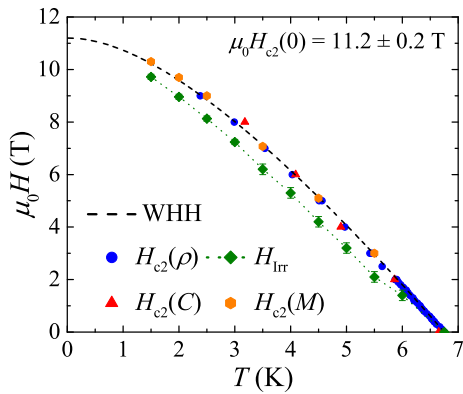


FIG. 7: Upper critical field versus temperature of Re_6Zr determined from the electrical resistivity, heat capacity, and magnetization data. The black curve shows the prediction for $H_{c2}(T)$ from the WHH model. For comparison $H_{\text{irr}}(T)$ from Fig. 5(b) is included. $H_{\text{irr}}(T)$ can be seen to diverge away from $H_{c2}(T)$ close to T_c and then stay a constant distance from $H_{c2}(T)$ down to 1.5 K.

with the values reported in Refs. 34 and 43. A fit was also attempted using a two-gap model, but it was found that $\Delta_0/k_B T_c$ for the two gaps iterated to the same value, indicating that the material has a single gap.

To determine whether the superconducting gap is isotropic (exponential) or anisotropic (power law) it is necessary to determine the temperature dependence of the electronic component of the heat capacity down to low temperature, as shown in Fig. 6(b). Due to the difficulties in approximating the zero-field hyperfine contribution in the specific heat this contribution has also been included in Fig. 6(b). Figure 6(b) shows fits to several power laws of the form $b \times T^N$, where b is a constant. Setting $N = 2$ or 3 the fits are poor, while $N = 5.8$ gives a good fit to the data, although this provides no physical insight. The $(C_{\text{el}} + C_{\text{hf}})$ data are best described by an exponential temperature dependence, suggesting an isotropic fully gapped s -wave BCS superconductor. To obtain the true nature of the superconducting gap heat-capacity data well below $T_c/10$ need to be analyzed⁴⁸. From Fig. 6(a) it can be seen that the specific heat is rather low. A more complete understanding of the hyperfine term is required to make any further progress with this analysis. Nuclear quadrupole measurements have also been performed on Re_6Zr and provide further evidence of a conventional BCS gap symmetry⁵⁰.

E. Upper critical field

In order to measure the upper critical field as a function of temperature $H_{c2}(T)$, the shift in T_c in magnetic fields of up to 9 T was determined from heat-capacity and resistivity data.

Figure 7 shows how H_{c2} varies with T . At temperatures just below T_c it is clear that H_{c2} increases linearly

with decreasing T , and this indicates that the temperature dependence of H_{c2} given by the Ginzburg-Landau formula is not appropriate. Instead, the Werthamer-Helfand-Hohenberg (WHH) model was used. This allows $H_{c2}(0)$ to be calculated in terms of the spin-orbit scattering and Pauli spin paramagnetism⁵¹, as it is expected that spin-orbit coupling may be strong due to the presence of the rhenium. $H_{c2}(T)$ can be found by solving

$$\ln\left(\frac{1}{t}\right) = \left(\frac{1}{2} + \frac{i\lambda_{\text{so}}}{4\gamma}\right) \psi\left(\frac{1}{2} + \frac{\bar{h} + \frac{1}{2}\lambda_{\text{so}} + i\gamma}{2t}\right) + \left(\frac{1}{2} - \frac{i\lambda_{\text{so}}}{4\gamma}\right) \psi\left(\frac{1}{2} + \frac{\bar{h} + \frac{1}{2}\lambda_{\text{so}} + i\gamma}{2t}\right) - \psi\left(\frac{1}{2}\right), \quad (10)$$

where $t = T/T_c$, λ_{so} is the spin-orbit scattering parameter, α_M is the Maki parameter, ψ is the digamma function, \bar{h} is the dimensionless form of the upper critical field given by

$$\bar{h} = \frac{4H_{c2}}{\pi^2} \left(\frac{dH_{c2}}{dT}\right)_{t=1}^{-1}, \quad (11)$$

and $\gamma = \sqrt{(\alpha\bar{h})^2 - (\frac{1}{2}\lambda_{\text{so}})^2}$. It is estimated that $\mu_0 H_{c2}(0) = (11.2 \pm 0.2)$ T, close to the value reported by Ref. 34 but below the Pauli paramagnetic limiting field $\mu_0 H_{\text{Pauli}}$ of (12.35 ± 0.09) T.

The WHH expression has three variables: the Maki parameter α_M , the spin-orbit scattering parameter λ_{so} , and the gradient at T_c . In their original work⁵¹, WHH state that α_M is not an adjustable parameter and needs to be obtained from experimental data; thus, α_M was not varied during the fitting.

The Maki parameter can be estimated experimentally by using the WHH expression

$$\alpha_M = \sqrt{2} \frac{H_{c2}^{\text{orb}}(0)}{H_{c2}^{\text{Pauli}}(0)}, \quad (12)$$

where H_{c2}^{orb} is the orbital limiting field given by

$$H_{c2}^{\text{orb}}(0) = -\alpha T_c \left. \frac{-dH_{c2}(T)}{dT} \right|_{T=T_c}, \quad (13)$$

where α is the purity factor, which for superconductors in the dirty limit is 0.693. The initial slope $-dH_{c2}(T)/dT|_{T=T_c}$ was found to be 2.44 T/K, giving $\mu_0 H_{c2}^{\text{orb}}(0) = (11.41 \pm 0.05)$ T. From Eq. (12) we obtain $\alpha_M = 1.31$, and the relative size of the Maki parameter indicates that the Pauli limiting field is non-negligible. Fixing $\alpha_M = 1.31$ produced $\lambda_{\text{so}} = 18 \pm 5$. It was found that this model is highly dependent on the starting values as an equally good fit, as judged by the reduced χ^2 , could be obtained by allowing the Maki parameter to vary. α_M was found to drift towards zero in nearly all cases along with λ_{so} , which would also tend to zero when allowed to vary. Unsurprisingly, the initial gradient

$-dH_{c2}(T)/dT|_{T=T_c}$ was found to remain constant within error.

In the first case with α_M fixed, the value for the spin-orbit term seems unusually large. There are several reasons why the WHH model may misrepresent what is happening in the system: (1) *Two-gap superconductor*. While the analysis of the superconducting gap was assumed to be a single gap it is possible that Re_6Zr is a two-gap superconductor where the gaps are of a similar magnitude, and this would give rise to some enhancement of H_{c2} ⁵². (2) *Granularity*. The polycrystalline sample of Re_6Zr will contain grain boundaries. The upper critical field will be increased above the bulk value once the grain size becomes smaller than the coherence length⁵³ (the grain size is unknown, so contributions from this source are unclear). (3) *Spin-orbit coupling*. Strong spin-orbit coupling effects can yield large enhancements of H_{c2} such that the temperature dependence of H_{c2} can become linear, although in the dirty limit this enhancement should be weaker⁵⁴. In order to obtain a more accurate value for $\mu_0 H_{c2}(0)$ high-field, low-temperature measurements of H_{c2} are needed in order to determine the form of the $\mu_0 H_{c2}(T)$ curve much closer to $T = 0$ K.

F. Properties of the superconducting state

The results of resistivity, heat-capacity, and magnetization measurements can now be combined in order to estimate some of the important superconducting properties of Re_6Zr . The Ginzburg-Landau coherence length $\xi_{\text{GL}}(0)$ can be estimated using $\mu_0 H_{c2}(0)$ from⁵⁵

$$H_{c2}(0) = \frac{\Phi_0}{2\pi\xi_{\text{GL}}^2(0)}, \quad (14)$$

where $\Phi_0 = 2.07 \times 10^{-15}$ Wb is the magnetic flux quantum. We calculate $\xi_{\text{GL}}(0) = (5.37 \pm 0.09)$ nm. $\mu_0 H_{c1}(0)$ and $\xi_{\text{GL}}(0)$ can be used to calculate the Ginzburg-Landau penetration depth $\lambda_{\text{GL}}(0)$ from the relation

$$H_{c1}(0) = \left(\frac{\Phi_0}{4\pi\lambda_{\text{GL}}^2(0)} \right) \ln \left(\frac{\lambda_{\text{GL}}(0)}{\xi_{\text{GL}}(0)} \right). \quad (15)$$

Using $\mu_0 H_{c1} = 10.3$ mT and $\xi_{\text{GL}}(0) = 5.37$ nm, we calculated $\lambda_{\text{GL}}(0) = (247 \pm 4)$ nm. The Ginzburg-Landau parameter can now be calculated by the relation

$$\kappa_{\text{GL}} = \frac{\lambda_{\text{GL}}(0)}{\xi_{\text{GL}}(0)}. \quad (16)$$

This yields a value of $\kappa_{\text{GL}} = 46.2 \pm 0.8$. For a superconductor to be classed as a type-II superconductor $\kappa_{\text{GL}} \geq \frac{1}{\sqrt{2}}$. It is clear that Re_6Zr is a strong type-II superconductor.

The thermodynamic critical field H_c can be calculated using $\xi_{\text{GL}}(0)$ and $\lambda_{\text{GL}}(0)$ using the relation

$$H_c^{\text{cal}}(0) = \frac{\Phi_0}{2\sqrt{2}\pi\xi_{\text{GL}}(0)\lambda_{\text{GL}}(0)}, \quad (17)$$

from this $H_c^{\text{cal}}(0)$ is estimated to be (175 ± 3) mT. The thermodynamic critical field can be experimentally estimated from the difference between the free energies per unit volume of the superconducting and normal states ΔF by⁵⁵

$$\frac{H_c^2(T)}{8\pi} = \Delta F = \int_{T_c}^T \int_{T_c}^{T'} \frac{C_s - C_n}{T''} dT'' dT', \quad (18)$$

where C_s and C_n are the heat capacities per unit volume. From Eq. (18) we obtain $H_c^{\text{exp}}(0) = (130 \pm 2)$ mT.

In order to calculate the electronic mean free path and London penetration depth in Re_6Zr the Sommerfeld coefficient can be written as⁵⁶

$$\gamma_n = \left(\frac{\pi}{3} \right)^{2/3} \frac{k_B^2 m^* V_{\text{f.u.}} n^{1/3}}{\hbar^2 N_A}, \quad (19)$$

where k_B is the Boltzmann constant, N_A is the Avogadro constant, $V_{\text{f.u.}}$ is the volume of a formula unit, m^* is the effective mass of quasiparticles, and n is the quasiparticle number density per unit volume. The electronic mean free path ℓ_e can be estimated from the residual resistivity ρ_0 by the equation

$$\ell_e = \frac{3\pi^2 \hbar^3}{e^2 \rho_0 m^* \nu_F^2}, \quad (20)$$

where the Fermi velocity ν_F is related to the effective mass and the carrier density by

$$n = \frac{1}{3\pi^2} \left(\frac{m^* \nu_F}{\hbar} \right)^3. \quad (21)$$

In the dirty limit the penetration depth is given by

$$\lambda_{\text{GL}}(0) = \lambda_L \left(1 + \frac{\xi_0}{\ell_e} \right)^{1/2}, \quad (22)$$

where ξ_0 is the BCS coherence length and λ_L is the London penetration depth, which is given by

$$\lambda_L = \left(\frac{m^*}{\mu_0 n e^2} \right)^{1/2}. \quad (23)$$

The Ginzburg-Landau coherence length is also affected in the dirty limit. The relationship between the BCS coherence length ξ_0 and the Ginzburg-Landau coherence ξ_{GL} at $T = 0$ is

$$\frac{\xi_{\text{GL}}(0)}{\xi_0} = \frac{\pi}{2\sqrt{3}} \left(1 + \frac{\xi_0}{\ell_e} \right)^{-1/2}. \quad (24)$$

Equations (19) - (24) form a system of four equations. To estimate the parameters m^* , n , ℓ_e , and ξ_0 this system of equations can be solved simultaneously using the values $\gamma_n = 26.9$ mJ mol⁻¹ K⁻², $\xi_{\text{GL}} = 5.37$ nm, and $\rho_0 = 142 \mu\Omega$ cm. For comparison, two values of λ_{GL} have been used; 247 nm is taken from Eq. (15), and 356 nm is taken from the μSR study in Ref. 34. The

TABLE I: Comparison of electronic properties of Re_6Zr for $\lambda_{\text{GL}}(H_{c1})$ and $\lambda_{\text{GL}}(\mu\text{SR})$.

Property	Units	H_{c1}	μSR
$\lambda_{\text{GL}}(0)$	nm	247	356
m^*/m_e		10.1 ± 0.1	12.9 ± 0.02
m_{band}^*/m_e		6.0 ± 0.1	7.7 ± 0.1
n	10^{27}m^{-3}	15.2 ± 0.2	7.4 ± 0.1
ξ_0	nm	3.28 ± 0.5	3.70 ± 0.05
ℓ_e	nm	1.45 ± 0.02	2.36 ± 0.03
ξ_0/ℓ_e		2.25 ± 0.03	1.56 ± 0.02
λ_{L}	nm	136 ± 2	222 ± 3
ν_{F}	m s^{-1}	88000 ± 1000	54000 ± 800
T_{F}	K	2570 ± 40	1240 ± 20
T_c/T_{F}		0.0026 ± 0.0001	0.0054 ± 0.0001

results are shown in Table I. From the mean free path ℓ_e calculated in Eq. (20) and ξ_0 calculated in Eq. (24), it is clear that $\xi_0 > \ell_e$, indicating that Re_6Zr is in the dirty limit. We find that these values are in close agreement with those previously reported for Re_6Zr ⁴³.

The bare-band effective mass m_{band}^* can be related to m^* , which contains enhancements from the many-body electron-phonon interactions⁵⁷

$$m^* = m_{\text{band}}^* (1 + \lambda_{\text{el-ph}}), \quad (25)$$

where $\lambda_{\text{el-ph}}$ is the electron-phonon coupling constant. The electron-phonon coupling constant gives the strength of the interaction between electron and phonons in superconductors. This can be estimated from McMillan's theory⁵⁸ from Θ_{D} and T_c ,

$$\lambda_{\text{el-ph}} = \frac{1.04 + \mu^* \ln(\Theta_{\text{D}}/1.45T_c)}{(1 - 0.62\mu^*) \ln(\Theta_{\text{D}}/1.45T_c) - 1.04}, \quad (26)$$

where μ^* is the repulsive screened Coulomb parameter, which can have a value between 0.1 and 0.15 but for intermetallic superconductors a value of 0.13 is typically used. Using T_c and Θ_{D} taken from Fig. 2(b), a value of $\lambda_{\text{el-ph}} = 0.67 \pm 0.02$ is obtained, suggesting this a moderately coupled superconductor. Using this value of $\lambda_{\text{el-ph}}$ and Eq. (25) a value for m_{band}^* can be found, as seen in Table I. Recently, these parameters have also been determined for the related compound Re_6Hf ^{36,37}. By substituting Zr by Hf the spin-orbit coupling should be enhanced, and it was hoped that this would provide an increase in the contribution of the spin-triplet component in the superconducting ground state. From the measurements performed in Refs. 36 and 37 it is clear that Re_6Hf and Re_6Zr are very similar and that the spin-orbit-coupling strength seems to have little effect on the properties of polycrystalline samples at least. Uemura *et*

 TABLE II: Normal-state and superconducting properties of Re_6Zr .

Re_6Zr property	Units	Value
T_c	K	6.75 ± 0.05
ρ_0	$\mu\Omega \text{ cm}$	142 ± 2
ρ_{sat}	$\mu\Omega \text{ cm}$	167 ± 1
Θ_{R} (from resistivity)	K	237 ± 2
Θ_{D} (from Sommerfeld coefficient)	K	338 ± 9
Θ_{D} (from Debye-Einstein fit)	K	258 ± 1
T_{E}	K	652 ± 12
γ_{n}	$\text{mJ mol}^{-1}\text{K}^{-2}$	26.9 ± 0.1
β_3	$\text{mJ mol}^{-1}\text{K}^{-4}$	0.35 ± 0.02
β_5	$\mu\text{J mol}^{-1}\text{K}^{-6}$	1.6 ± 0.1
$\lambda_{\text{el-ph}}$		0.67 ± 0.02
$\Delta C/\gamma_{\text{n}}T_c$		1.60 ± 0.02
$\Delta_0/k_{\text{B}}T_c$		1.86 ± 0.05
$\mu_0 H_{c1}(0)$	mT	10.3 ± 0.1
$\mu_0 H_{c2}(0)$	T	11.2 ± 0.2
$\mu_0 H_{\text{c}}^{\text{cal}}(0)$	mT	175 ± 3
$\mu_0 H_{\text{c}}^{\text{exp}}(0)$	mT	130 ± 2
$\mu_0 H_{\text{c}2}^{\text{orbital}}(0)$	T	11.41 ± 0.05
$\mu_0 H_{\text{c}2}^{\text{Pauli}}(0)$	T	12.35 ± 0.09
$\xi_{\text{GL}}(0)$	nm	5.37 ± 0.09
$\lambda_{\text{GL}}(0)$	nm	247 ± 4
$\kappa_{\text{GL}}(0)$		46.2 ± 0.8

al. have described a method for classifying superconductors based on the ratio of the critical temperature T_c to the effective Fermi temperature T_{F} ⁵⁹. The values of m^* and n taken from Table I can be used to calculate an effective Fermi temperature for Re_6Zr using

$$k_{\text{B}}T_{\text{F}} = \frac{\hbar^2}{2m^*} (3\pi^2 n)^{2/3}, \quad (27)$$

and the result is presented in Table I. It has been observed that the high- T_c , organic, heavy-fermion, and other unconventional superconductors lie in the range $0.01 \leq T_c/T_{\text{F}} \leq 0.1$ ⁵⁹⁻⁶¹. However, Re_6Zr lies outside of the range for unconventional superconductivity, supporting the view that the superconducting mechanism is primarily conventional.

IV. SUMMARY

In summary, single-phase polycrystalline samples of Re_6Zr were prepared by the arc-melting technique. Powder x-ray diffraction data confirmed the cubic, noncentrosymmetric α -Mn crystal structure and the phase pu-

rity of the samples. The normal-state and superconducting properties of Re_6Zr were studied using magnetization, heat-capacity, and resistivity measurements. We have established that Re_6Zr is a moderately coupled superconductor with a transition at $T_c = (6.75 \pm 0.05)$ K. In the normal state, resistivity measurements show that Re_6Zr has poor metallic behavior that is dominated by disorder. We showed that it is possible to fit these data with a parallel-resistor model that considers contributions in addition to the electron-phonon interactions. Specific-heat measurements of the normal state reveal no indication of any structural phase transitions down to low temperature and were fit using a simple Debye-Einstein function. The jump in specific heat at T_c is $\Delta C/\gamma_n T_c = 1.60 \pm 0.02$, while $C(T)$ below T_c was fit using the BCS model, giving $\Delta_0/k_B T_c = 1.86 \pm 0.05$. Both values are well above those expected for a conventional BCS superconductor, suggesting the electron-phonon coupling is enhanced in this system. The mean free path ℓ_e is estimated to be (1.45 ± 0.02) nm. The best approximation for $H_{c2}(0)$ was found using the WHH model. From $H_{c2}(0)$ the coherence length was calculated with $\xi_{\text{GL}}(0) = (5.37 \pm 0.09)$ nm, confirming that Re_6Zr is in the dirty limit. Using the magnetization data, it was possible to estimate $\mu_0 H_{c1}(0) = (10.3 \pm 0.1)$ mT and so calculate the penetration depth $\lambda_{\text{GL}}(0) = (247 \pm 4)$ nm. The Ginzburg-Landau coefficient $\kappa_{\text{GL}}(0) = 46.2 \pm 0.8$

confirmed that Re_6Zr is a strong type-II superconductor. A summary of all the experimentally measured and estimated parameters is given in Table II. From our measurements we can conclude the superconducting order parameter is well described by an isotropic gap with s -wave pairing symmetry and enhanced electron-phonon coupling, despite the observation of spontaneous magnetization associated with TRS breaking being observed at temperatures below the superconducting transition in previous work³⁴. This suggests Re_6Zr has a superconducting ground state that features a dominant s -wave component, while the exact nature of the triplet component is undetermined. In order to determine if the superconductivity is nonunitary, further experimental work on high-quality single crystals, as well as further analysis of “clean” and “dirty” samples to examine the role grain boundaries and impurities play in determining the superconducting behavior of Re_6Zr , is vital.

Acknowledgments

This work is funded by the EPSRC, United Kingdom, through Grants No. EP/I007210/1 and No. EP/M028771/1.

* d.mayoh@warwick.ac.uk

† Present address: Paul Scherrer Institut, 5232 Villigen PSI, Switzerland

‡ m.r.lees@warwick.ac.uk

¹ E. Bauer, G. Hilscher, H. Michor, C. Paul, E. W. Scheidt, A. Griбанov, Y. Seropegin, H. Noel, M. Sigrist, and P. Rogl, *Phys. Rev. Lett.* **92**, 027003 (2004).

² E. Bauer, H. Kaldarar, A. Prokofev, E. Royanian, A. Amato, J. Sereni, W. Bramer-Escamilla, and I. Bonalde, *J. Phys. Soc. Jpn.* **76**, 051009 (2007).

³ E. Bauer and M. Sigrist, *Non-centrosymmetric superconductors: introduction and overview* (Heidelberg, Springer-Verlag, 2012).

⁴ E. I. Rashba, *Sov. Phys. Solid State* **2**, 1109 (1960).

⁵ L. P. Gorkov and E. I. Rashba, *Phys. Rev. Lett.* **87**, 037004 (2001).

⁶ Z. Sun, M. Enayat, A. Maldonado, C. Lithgow, E. Yelland, D. C. Peets, A. Yaresko, A. P. Schnyder, and P. Wahl, *Nat. Commun.* **6**, 6633 (2015).

⁷ S. Guan, P. Chen, M. Chu, R. Sankar, F. Chou, H. Jeng, C. Chang, and T. Chuang, *Sci. Adv.* **2**, 1600894 (2016).

⁸ H. Q. Yuan, D. F. Agterberg, N. Hayashi, P. Badica, D. Vandervelde, K. Togano, M. Sigrist, and M. B. Salamon, *Phys. Rev. Lett.* **97**, 017006 (2006).

⁹ M. Nishiyama, Y. Inada, and G.-Q. Zheng, *Phys. Rev. Lett.* **98**, 047002 (2007).

¹⁰ H. Takeya, M. ElMassalami, S. Kasahara, and K. Hirata, *Phys. Rev. B* **76**, 104506 (2007).

¹¹ S. Harada, J. J. Zhou, Y. G. Yao, Y. Inada, and G.-Q. Zheng, *Phys. Rev. B* **86**, 220502 (2012).

¹² A. B. Karki, Y. M. Xiong, I. Vekhter, D. Browne, P. W. Adams, D. P. Young, K. R. Thomas, J. Y. Chan, H. Kim, and R. Prozorov, *Phys. Rev. B* **82**, 064512 (2010).

¹³ P. K. Biswas, M. R. Lees, A. D. Hillier, R. I. Smith, W. G. Marshall, and D. M. Paul, *Phys. Rev. B* **84**, 184529 (2011).

¹⁴ G. Eguchi, D. C. Peets, M. Kriener, Y. Maeno, E. Nishibori, Y. Kumazawa, K. Banno, S. Maki, and H. Sawa, *Phys. Rev. B* **83**, 024512 (2011).

¹⁵ V. K. Anand, A. D. Hillier, D. T. Adroja, A. M. Strydom, H. Michor, K. A. McEwen, and B. D. Rainford, *Phys. Rev. B* **83**, 064522 (2011).

¹⁶ A. B. Karki, Y. M. Xiong, N. Haldolaarachchige, I. Stadler, S. and Vekhter, P. W. Adams, D. P. Young, W. A. Phelan, and J. Y. Chan, *Phys. Rev. B* **83**, 144525 (2011).

¹⁷ J. Chen, M. B. Salamon, S. Akutagawa, J. Akimitsu, J. Singleton, J. L. Zhang, L. Jiao, and H. Q. Yuan, *Phys. Rev. B* **83**, 144529 (2011).

¹⁸ T. Klimczuk, F. Ronning, V. Sidorov, R. J. Cava, and J. D. Thompson, *Phys. Rev. Lett.* **99**, 257004 (2007).

¹⁹ A. Maisuradze, W. Schnelle, R. Khasanov, R. Gumeniuk, M. Nicklas, H. Rosner, A. Leithe-Jasper, Y. Grin, A. Amato, and P. Thalmeier, *Phys. Rev. B* **82**, 024524 (2010).

²⁰ G. M. Luke, Y. Fudamoto, K. M. Kojima, M. I. Larkin, J. Merrin, B. Nachumi, Y. J. Uemura, Y. Maeno, Z. Q. Mao, Y. Mori, H. Nakamura, and M. Sigrist, *Nature (London)* **394**, 558 (1998).

²¹ J. Xia, Y. Maeno, P. T. Beyersdorf, M. M. Fejer, and A. Kapitulnik, *Phys. Rev. Lett.* **97**, 167002 (2006).

²² Y. Aoki, A. Tsuchiya, T. Kanayama, S. R. Saha, H. Sugawara, H. Sato, W. Higemoto, A. Koda, K. Ohishi,

- K. Nishiyama, and R. Kadono, *Phys. Rev. Lett.* **91**, 067003 (2003).
- ²³ L. Shu, W. Higemoto, Y. Aoki, A. D. Hillier, K. Ohishi, K. Ishida, R. Kadono, A. Koda, O. O. Bernal, D. E. MacLaughlin, Y. Tunashima, Y. Yonezawa, S. Sanada, D. Kikuchi, H. Sato, H. Sugawara, T. U. Ito, and M. B. Maple, *Phys. Rev. B* **83**, 100504(R) (2011).
- ²⁴ G. M. Luke, A. Keren, L. P. Le, W. D. Wu, Y. J. Uemura, D. A. Bonn, L. Taillefer, and J. D. Garrett, *Phys. Rev. Lett.* **71**, 1466 (1993).
- ²⁵ P. D. de Reotier, A. Huxley, A. Yaouanc, J. Flouquet, P. Bonville, P. Impert, P. Pari, P. C. M. Gubbens, and A. M. Mulders, *Phys. Lett. A* **205**, 239 (1995).
- ²⁶ W. Higemoto, K. Satoh, N. Nishida, A. Koda, K. Nagamine, Y. Haga, E. Yamamoto, N. Kimura, and Y. Onuki, *Physica (Amsterdam)* **281B-282B**, 984 (2000).
- ²⁷ R. H. Heffner, J. L. Smith, J. O. Willis, P. Birrer, C. Baines, F. N. Gygax, B. Hitti, E. Lippelt, H. R. Ott, A. Schenck, E. A. Knetsch, J. A. Mydosh, and D. E. MacLaughlin, *Phys. Rev. Lett.* **65**, 2816 (1990).
- ²⁸ A. D. Hillier, J. Quintanilla, B. Mazidian, J. F. Annett, and R. Cywinski, *Phys. Rev. Lett.* **109**, 097001 (2012).
- ²⁹ A. Bhattacharyya, D. T. Adroja, J. Quintanilla, A. D. Hillier, N. Kase, A. M. Strydom, and J. Akimitsu, *Phys. Rev. B* **91**, 060503 (2015).
- ³⁰ A. D. Hillier, J. Quintanilla, and R. Cywinski, *Phys. Rev. Lett.* **102**, 117007 (2009).
- ³¹ J. Quintanilla, A. D. Hillier, J. F. Annett, and R. Cywinski, *Phys. Rev. B* **82**, 174511 (2010).
- ³² J. A. T. Barker, D. Singh, A. Thamizhavel, A. D. Hillier, M. R. Lees, G. Balakrishnan, D. M. Paul, and R. P. Singh, *Phys. Rev. Lett.* **115**, 267001 (2015).
- ³³ B. T. Matthias, V. B. Compton, and E. Corenzwit, *J. Phys. Chem. Solids* **19**, 130 (1961).
- ³⁴ R. P. Singh, A. D. Hillier, B. Mazidian, J. Quintanilla, J. F. Annett, D. M. Paul, G. Balakrishnan, and M. R. Lees, *Phys. Rev. Lett.* **112**, 107002 (2014).
- ³⁵ A. Aharoni, *J. Appl. Phys.* **83**, 3432 (1998).
- ³⁶ D. Singh, A. D. Hillier, A. Thamizhavel, and R. P. Singh, *Phys. Rev. B* **94**, 054515 (2016).
- ³⁷ B. Chen, Y. Guo, H. Wang, Q. Su, Q. Mao, J. Du, Y. Zhou, J. Yang, and M. Fang, *Phys. Rev. B* **94**, 024518 (2016).
- ³⁸ C. S. Lue, H. F. Liu, C. N. Kuo, P. S. Shih, J.-Y. Lin, Y. K. Kuo, M. W. Chu, H. T-L, and Y. Y. Chen, *Superconduct. Sci. Tech.* **26**, 055011 (2013).
- ³⁹ B. Joshi, A. Thamizhavel, and S. Ramakrishnan, *Phys. Rev. B* **84**, 064518 (2011).
- ⁴⁰ Z. Fisk and G. W. Webb, *Phys. Rev. Lett* **36**, 1084 (1976).
- ⁴¹ H. Wiesmann, M. Gurvitch, H. Lutz, A. K. Ghosh, B. Schwarz, M. Strongin, P. B. Allen, and J. W. Halley, *Phys. Rev. Lett* **38**, 782 (1977).
- ⁴² G. Grimvall, *The Electron-Phonon Interaction in Metals* (North-Holland Publishing Company, 1981).
- ⁴³ M. A. Khan, A. B. Karki, T. Samanta, D. Browne, S. Stadler, I. Vekhter, A. Pandey, P. W. Adams, D. P. Young, S. Teknowijoyo, K. Cho, R. Prozorov, and D. E. Graf, *Phys. Rev. B* **94**, 144515 (2016).
- ⁴⁴ E. S. R. Gopal, *Specific Heats at Low Temperatures* (Plenum, New York, 1966).
- ⁴⁵ P. H. Keesom and C. A. Bryant, *Phys. Rev. Lett.* **2**, 260 (1959).
- ⁴⁶ D. R. Smith and P. H. Keesom, *Phys. Rev. B* **1**, 188 (1970).
- ⁴⁷ J. Chen, L. Jiao, J. L. Zhang, Y. Chen, L. Yang, M. Nicklas, F. Steglich, and H. Q. Yuan, *Phys. Rev. B* **88**, 144510 (2013).
- ⁴⁸ B. Mazidian, J. Quintanilla, A. D. Hillier, and J. F. Annett, *Phys. Rev. B* **88**, 224504 (2013).
- ⁴⁹ B. Muhlschlegel, *Z. Phys.* **155**, 313 (1959).
- ⁵⁰ K. Matano, R. Yatagai, S. Maeda, and G. Q. Zheng, *Phys. Rev. B* **94**, 214513 (2016).
- ⁵¹ N. R. Werthamer, E. Helfand, and P. C. Hohenberg, *Phys. Rev.* **147**, 295 (1966).
- ⁵² A. Gurevich, *Phys. Rev. B* **67**, 184515 (2003).
- ⁵³ P. deGennes and M. Tinkham, *Physics* **1**, 107 (1964).
- ⁵⁴ J. P. Carbotte, *Rev. Mod. Phys.* **62**, 1027 (1990).
- ⁵⁵ C. P. Poole, A. F. Horacio, and J. C. Richard, *Superconductivity* (Academic Press, 1995).
- ⁵⁶ C. Kittel, *Introduction to Solid State Physics*, 3rd ed. (John Wiley & Sons, 1967).
- ⁵⁷ G. Grimval, *Phys. Scr.* **14**, 63 (1976).
- ⁵⁸ W. L. McMillan, *Phys. Rev.* **167**, 331 (1968).
- ⁵⁹ Y. J. Uemura, L. P. Le, G. M. Luke, B. J. Sternlieb, W. D. Wu, J. H. Brewer, T. M. Riseman, C. L. Seaman, M. B. Maple, M. Ishikawa, D. G. Hinks, J. D. Jorgensen, G. Saito, and H. Yamochi, *Phys. Rev. Lett* **66**, 2665 (1991).
- ⁶⁰ Y. J. Uemura, V. J. Emery, A. R. Moodenbaugh, M. Suenaga, D. C. Johnston, A. J. Jacobson, J. T. Lewandowski, J. H. Brewer, R. F. Kiefl, S. R. Kreitzman, G. M. Luke, T. Riseman, C. E. Stronach, W. J. Kossler, J. R. Kempton, X. H. Yu, D. Opie, and H. E. Schone, *Phys. Rev. B* **38**, 909 (1988).
- ⁶¹ Y. J. Uemura, G. M. Luke, B. J. Sternlieb, J. H. Brewer, J. F. Carolan, W. N. Hardy, R. Kadono, J. R. Kempton, R. F. Kiefl, S. R. Kreitzman, P. Mulhern, T. M. Rise-man, D. L. Williams, B. X. Yang, S. Uchida, H. Takagi, J. Gopalakrishnan, A. W. Sleight, M. A. Subramanian, C. L. Chien, M. Z. Cieplak, G. Xiao, V. Y. Lee, B. W. Statt, C. E. Stronach, W. J. Kossler, and X. H. Yu, *Phys. Rev. Lett* **62**, 2317 (1989).